



OPEN Evolution of surrounding rock distortion energy during closely spaced coal seam mining and innovative coal pillar design method

Zhaolong Li^{1,2}✉, Jun Li¹, Renliang Shan², Jingju Liu³, Xiao Tong⁴ & Nan Liu¹

This article innovatively examines the selection of the optimal width of the upper coal pillar during the mining of closely spaced coal seams geological conditions based on the engineering failure analysis of stress deviator (distortion energy density index). A theoretical calculation formula for the stress deviator of the surrounding rock at the coal pillar floor is derived. Analysis of the theoretical formula reveals that the load magnitude on the coal pillar and the width of the coal pillar (D) are the primary factors influencing the distribution characteristics of the stress deviator at the coal pillar floor. Theoretical and numerical research consistently demonstrates the distribution characteristics of stress deviator in the bottom plate of coal pillar. The area of stress deviator concentration on the coal pillar floor is primarily situated at the boundary of the coal pillar, gradually diminishing as the horizontal distance from the coal pillar and the depth of the surrounding rock increase. The overall distribution of the stress deviator exhibits a symmetrical "Y-shaped" pattern. With a smaller coal pillar width (D), the influence range of the stress deviator decreases, but the concentration is more pronounced. As the coal pillar width increases, the concentration of stress deviator gradually diminishes, with a significant decrease in the peak value but an increase in the influence range. Based on the research findings regarding the distribution characteristics of stress deviator in the coal pillar floor, this article innovatively determines the optimal width of the upper coal pillar to be 20 m during the mining of closely spaced coal seams in the Malan Mine. To validate the accuracy and reliability of this research, additional simulation experiments and industrial experiments were conducted. The stress and strain fields of the surrounding rock in the simulation experiments, along with the results of on-site investigation and drilling observation, confirm that a coal pillar width of 20 m ensures stability.

Keywords Stress deviator, Coal pillar, Mining, Closely spaced coal seams, Distortion energy

Closely spaced coal seams constitute a prevalent geological condition, yet they entail considerable mining risks, with the majority of existing mining methods for such seams being downward oriented¹. However, mining of the upper coal seam will inevitably cause varying degrees of damage, deformation, and plastic damage to the lower coal seam. The collapse of the upper coal seam roof will also cause nonuniform stress distribution in various parts of the lower coal seam^{2,3}, which is extremely unfavorable for the mining of the lower coal seam. Therefore, many experts and scholars^{4–6} have paid attention to the stress distribution and plastic damage degree of the lower coal group during the downward mining process of closely spaced coal seams^{7,8}. In these cases, the layout of the upper panels and coal pillars has become the key factor affecting the stability of the surrounding rock in the mining area.

In traditional descending mining of closely spaced coal seams, residual coal pillars⁹ are left behind after upper coal seam extraction. The overburden pressure from the roof of the gob is transferred to the floor through these coal pillars, resulting in an uneven stress distribution^{10,11} in the floor beneath the pillars. If the coal pillar is

¹School of Civil Engineering, Hebei University of Engineering, Handan 056038, China. ²School of Mechanics and Civil Engineering, China University of Mining & Technology (Beijing), Beijing 100083, China. ³School of Landscape and Ecological Engineering, Hebei University of Engineering, Handan 056038, China. ⁴School of Earth Science and Engineering, Hebei University of Engineering, Handan 056038, China. ✉email: cumtblzl@163.com

undersized, it may lead to safety hazards during lower seam mining. Conversely, if the pillar is oversized, it can result in resource waste. Therefore, the rational design of the upper coal pillar size is critical for ensuring mining safety and maximizing resource recovery in closely spaced seam mining. Wang et al. (2025)¹² analyzed the vertical stress, strain, and plastic zone in the coal pillar area for different aspect ratios, and proposed a reasonable coal pillar width. Li et al. (2020)¹³ designed and arranged coal pillars based on the shape of the surrounding rock's plastic zone. Zhu et al. (2022)¹⁴ employed numerical simulations to determine the vertical stress and plastic zone in inclined coal seams, and accordingly optimized coal pillar design. He et al. (2019)¹⁵ focused on variations in tunnel surrounding rock stress, deformation, and plastic zone under different coal pillar widths to inform coal pillar design in mining roadways.

The above research results show that in the related research, the vertical stress below the residual coal pillar was considered the main parameter affecting the deformation and failure of the surrounding rock in response to the stability issue of the rock below residual coal pillar. The selection of coal pillar size is often based on work experience (The most common method of coal pillar design), vertical stress distribution, plastic zones. However, it cannot be denied that the rock mass below the coal pillar is a three-dimensional body with isotropic stress^{16–18}. While it is subjected to vertical stress, it will also be subjected to horizontal, shear, other isotropic stresses¹⁹ and distortion energy²⁰. Only considering vertical stress is insufficient. In elastic mechanics, stress deviator is the main cause of shape deformation in rock masses^{21,22}. The second invariant of the stress deviator, J_2 , is a comprehensive indicator that considers the isotropic stress uniformity of the surrounding rocks^{23–26}. It can represent the distortion energy density of rock masses and reflect their stability^{27–29}. Therefore, this paper characterizes the stress deviator with the second invariant J_2 of the stress deviator, through the study of the distribution characteristics of the second invariant J_2 of the stress deviator in the surrounding rock below a residual coal pillar, reveals the distortion energy causes of rock deformation and failure, which can resolve related engineering problems and enrich the theory of mining engineering failure analysis.

Project summary

The Malan Mine is located in the central part of Shanxi Province, China. The main coal seams currently being mined there are the #02 and #2 coal seams, with a distance of approximately 7 m between them. The thickness of the #02 coal seam in the upper layer is 2.1 m, and the corresponding roof and floor are sandy mudstone and mudstone, respectively. The thickness of the #2 coal seam in the lower layer is 2.2 m, and the corresponding roof and floor are sandy mudstone and siltstone, respectively. The two coal seams are buried at a depth of approximately 410 m, with a nearly horizontal dip angle. The stratigraphic column is shown in Fig. 1.

The 10605 panel is located in the #02 coal seam and has been mined. The 10607 panel is adjacent to the 10605 panel in the #02 coal seam at the same level. The layout of the panel is shown in Fig. 2.

#02 and #2 coal seams of Malan Mine exemplify typical closely spaced coal seams geological conditions, and they are being mined by downward mining. Therefore, after the mining of the 10605 and 10607 panels (In #02 coal seam), there will be obvious stress concentration areas below the coal pillar, causing irreversible plastic deformation and damage to the lower coal group (#2 coal seam). Therefore, a reasonable selection of the position and size of the coal pillar will play a decisive role in the stress state, stress deviator distribution, distortion energy evolution and elastic-plastic state of the surrounding rock before lower coal mining.

Thickness/m	Lithology	Strata	Rock features
6.05		Silty mudstone	Dark gray, thickly layered
2.14		#02 coal	Black, lumpy, poor lithology
4.97		Sandstone	Off-white medium-fine sandstone, mainly quartz and feldspar
0.45		#1 coal	Black, containing sandy mudstone
1.49		Silty mudstone	Dark gray, containing pyrite film
2.20		#2 coal	Black, semibright coal, blocky
1.89		Siltstone	Gray, containing fossilized plant roots
0.49		#3 coal	Black, semibright coal, blocky
5.00		Silty mudstone	Dark gray

Fig. 1. Stratigraphic column of the rock strata.

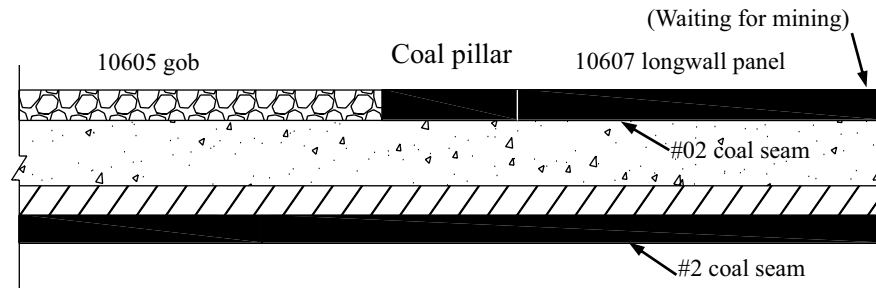
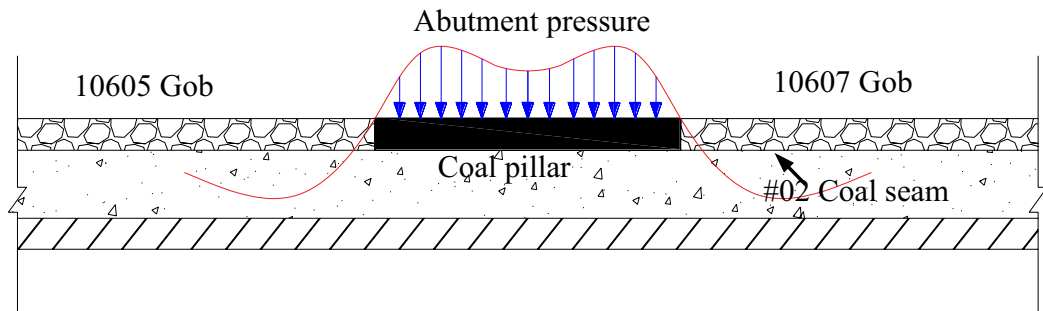
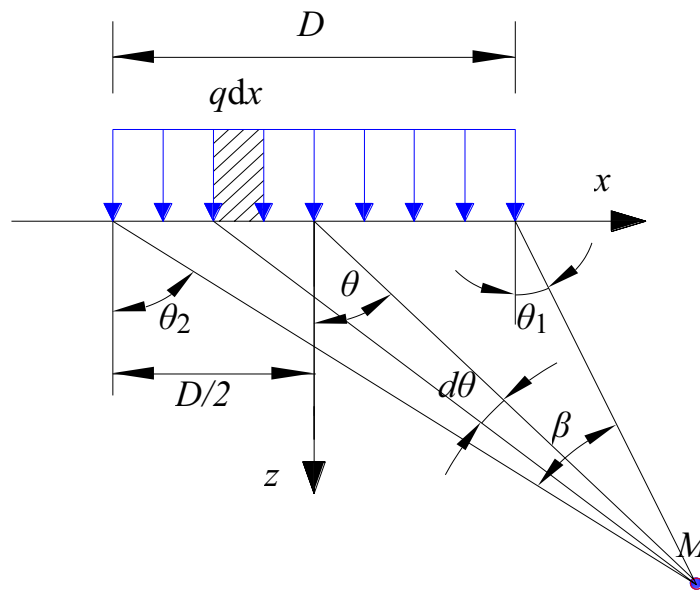


Fig. 2. Arrangement of the longwall panels.



(a) Abutment pressure distribution of coal pillar



(b) Simplified mechanical calculation model

Fig. 3. Calculation model of floor stress under a coal pillar.

**Theoretical calculation of the stress deviator
Stress analysis of the coal pillar floor**

According to mine pressure theory, after coal seam mining, the roof rock will be fragmented, and the stress of the overburden in the gob cannot be directly transmitted to the floor. Therefore, the stress near the residual coal pillar will concentrate after stress redistribution, as shown in Fig. 3a.

In theoretical calculations, the load at the coal pillar is simplified as a uniformly distributed load, as shown in Fig. 3b. q represents the uniformly distributed load acting on the floor of the coal pillar, D represents the width of the uniformly distributed load, and angle β is formed by the line connecting the boundary points on both sides of the load and point M . dx represents a microscale increment of the load length, and $d\theta$ is a microscale increment of the angle between the load and point M . σ_x , σ_z , and τ_{xz} represent the horizontal, vertical, and shear stresses at point M under uniformly distributed loads.

According to the integration calculation results, the formula for calculating the stress parameters inside the floor layer under uniformly distributed loads is^{30,31}:

$$\sigma_x = \frac{q}{\pi} \left[\arctan \frac{x + D/2}{z} - \arctan \frac{x - D/2}{z} - \frac{z(x + D/2)}{(x + D/2)^2 + z^2} + \frac{z(x - D/2)}{(x - D/2)^2 + z^2} \right] \tag{1}$$

$$\sigma_z = \frac{q}{\pi} \left[\arctan \frac{x + D/2}{z} - \arctan \frac{x - D/2}{z} + \frac{z(x + D/2)}{(x + D/2)^2 + z^2} - \frac{z(x - D/2)}{(x - D/2)^2 + z^2} \right] \tag{2}$$

$$\tau_{xz} = -\frac{q}{\pi} \left[\frac{z^2}{(x + D/2)^2 + z^2} + \frac{z^2}{(x - D/2)^2 + z^2} \right] \tag{3}$$

Calculation and derivation of the stress deviator in the coal pillar floor

The second invariant J_2 of the stress deviator represents the magnitude of the distortion energy and strain energy density of the rock mass, which is a comprehensive indicator of rock mass stability under isotropic stress conditions. It does not change with the selection of coordinate axes. However, the stress deviator of the coal pillar floor will change with the changes in various stress indicators, and its calculation expression is:

$$J_2 = - \left| \begin{matrix} \sigma_x - \sigma_0 & \tau_{xy} \\ \tau_{yx} & \sigma_y - \sigma_0 \end{matrix} \right| - \left| \begin{matrix} \sigma_y - \sigma_0 & \tau_{yz} \\ \tau_{zy} & \sigma_z - \sigma_0 \end{matrix} \right| - \left| \begin{matrix} \sigma_z - \sigma_0 & \tau_{zx} \\ \tau_{xz} & \sigma_x - \sigma_0 \end{matrix} \right| \tag{4}$$

$$= \frac{1}{6} [(\sigma_x - \sigma_y)^2 + (\sigma_y - \sigma_z)^2 + (\sigma_z - \sigma_x)^2 + 6(\tau_{xy}^2 + \tau_{yz}^2 + \tau_{zx}^2)]$$

$$\sigma_0 = \frac{1}{3}(\sigma_x + \sigma_y + \sigma_z) = \frac{1}{3}(\sigma_1 + \sigma_2 + \sigma_3) \tag{5}$$

In the above equation, σ_0 is the average stress. If the stress in the surrounding rock of the coal pillar floor is regarded as a two-dimensional plane problem, the y -direction stress perpendicular to the plane can be regarded as the intermediate principal stress. For ease of calculation, the y -direction stress is considered to have the same magnitude as the x -direction stress, and formula (5) is substituted into Eq. (4). The stress deviation J_2 can be expressed as:

$$J_2 = - \left| \begin{matrix} \frac{\sigma_x - \sigma_z}{3} & 0 \\ 0 & \frac{\sigma_x - \sigma_z}{3} \end{matrix} \right| - \left| \begin{matrix} \frac{\sigma_x - \sigma_z}{3} & 0 \\ 0 & \frac{2(\sigma_z - \sigma_x)}{3} \end{matrix} \right| - \left| \begin{matrix} \frac{2(\sigma_z - \sigma_x)}{3} & \tau_{zx} \\ \tau_{xz} & \frac{\sigma_x - \sigma_z}{3} \end{matrix} \right| \tag{6}$$

$$= \frac{1}{6} [2(\sigma_x - \sigma_z)^2 + 6\tau_{xz}^2] = \frac{1}{3} (\sigma_x - \sigma_z)^2 + \tau_{xz}^2$$

After substituting the calculated stress formulas (1), (2), and (3) into formula (6), the expression for calculating the stress deviator of the rock layer below the coal pillar under uniform loading can be obtained:

$$J_2 = \frac{4}{3} \left(\frac{q}{\pi}\right)^2 \left[\frac{z(x - D/2)}{(x - D/2)^2 + z^2} - \frac{z(x + D/2)}{(x + D/2)^2 + z^2} \right]^2 \tag{7}$$

$$+ \left(\frac{q}{\pi}\right)^2 \left[\frac{z^2}{(x + D/2)^2 + z^2} + \frac{z^2}{(x - D/2)^2 + z^2} \right]^2$$

According to Eq. (7), there are many factors that affect the distribution of the stress deviator in the coal pillar floor, including the load q at the coal pillar, the relative position of the action point M , and the width D of the coal pillar. q at the coal pillar is a mining pressure parameter, and the relative position of M is determined by the interlayer spacing of the closely spaced coal seams. These parameters are difficult to change during mining construction.

However, the width of the residual coal pillar in the upper coal seam during mining of the closely spaced coal seams can be designed. The width of the residual coal pillar will greatly affect the distribution of the stress deviator below the coal pillar and has a great impact on the elastic-plastic state of the lower coal seam before mining. Therefore, a reasonable design of the coal pillar width is of great significance for the stability of the surrounding rock during the mining of closely spaced coal seams.

The distribution of stress deviator in the coal pillar floor

Considering the load in the coal pillar area on site, the stress distribution curve at $z=5$ m below the coal pillar at $q=18$ MPa was selected for analysis, as shown in Fig. 4. The data selection takes into account the general applicability of closely spaced coal seam mining, field stress. Figure 4 shows the stress deviator distribution curve at 5 m below the coal pillar when the width of the coal pillar is $D=10$ m, $D=15$ m, $D=20$ m, and $D=25$ m. The

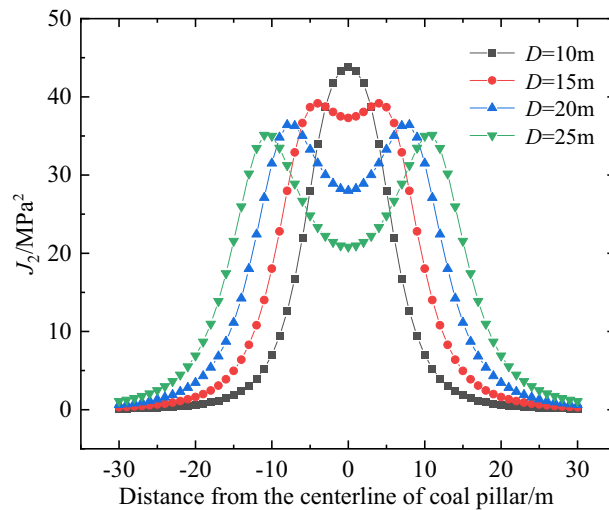


Fig. 4. Calculation results of the stress deviator below the coal pillar.

stress deviator distribution curves show a symmetrical distribution, with the coal pillar centerline as the axis of symmetry.

When the coal pillar is narrow ($D=10$ m), the stress deviator distribution curve shows a "single-peak" distribution, with a large J_2 peak, which appears at the center of the coal pillar. As the width of the coal pillar continues to increase, the stress deviator gradually presents a "double-peak" distribution form, the J_2 peak gradually decreases, and the peak point gradually moves toward both sides of the coal pillar.

As D increases, the peak point of the stress deviator in the floor rock layer gradually moves toward both sides of the coal pillar, and the peak point is roughly located at the edge of the coal pillar. The peak stress deviator of the surrounding rock below the coal pillar gradually decreases with increasing D , and the integrity and stability of the rock mass also improve.

J_2 represents the deformation energy of the rock mass. Physically, when J_2 reaches its peak, it indicates that the deformation energy of the rock mass has reached a maximum, corresponding to the maximum stress experienced in all directions. According to the Mises criterion, a greater difference in principal stresses leads to a higher J_2 value, indicating higher deformation energy and lower stability of the surrounding rock. Conversely, a lower J_2 value suggests greater rock mass stability.

Numerical calculation of the stress deviator

To further study the distribution characteristics of the stress deviator below the coal pillar and explore the stability state of the surrounding rock under different working conditions, this section establishes a numerical calculation model based on the distribution of rock layers near the 10607 panel of the Malan Mine and postprocesses the simulation results.

Numerical model

The model size is $x \times y \times z = 200 \text{ m} \times 20 \text{ m} \times 50 \text{ m}$, as shown in Fig. 5. The model includes 11 layers of rock, and the physical and mechanical parameters of each layer are shown in Table 1. The rock formation parameters are derived from the mine data and related mechanical experiments.

According to the stress test results of the Malan Mine, a vertical stress of 10 MPa is applied to the top of the model, with a horizontal lateral pressure coefficient $\lambda = 0.8$. The mining method is one-time excavation. $0 \leq x \leq 90$ is the range of the first panel. The range of the second panel is $100 \leq x \leq 200$, $110 \leq x \leq 200$, $120 \leq x \leq 200$ according to the width of the coal pillar. The horizontal displacement of the front, back, left, and right surfaces of the model are limited in the x and y directions, and the vertical displacement of the bottom is limited in the z direction, using the Mohr-Coulomb strength criterion for calculation.

Spatial distribution characteristics of stress deviator

The numerical model after coal seam mining is subjected to data postprocessing operations, and the stress deviator distribution in the coal pillar floor is obtained for different widths of the coal pillar. Due to space limitations, this section presents stress deviator contour plots for coal pillar widths of $D=10$ m, $D=20$ m, and $D=30$ m.

In Fig. 6, the stress deviator contour plots for different coal pillar widths use the same color scale. The distribution of the stress deviator in the floor of the double gob within ± 40 m from the centerline of the coal pillar is captured in the figure. The red and black dashed lines represent the positions of the roof and floor of the lower coal seam (#2 coal seam), respectively.

As shown in Fig. 6, when $\lambda = 0.8$, the area of stress deviator concentration is located below the coal pillar, while the unloading area of the stress deviator is located below the gob. These contour plots show that the stress deviator distribution below the coal pillar exhibits a symmetrical "Y-shaped" distribution. The main area of

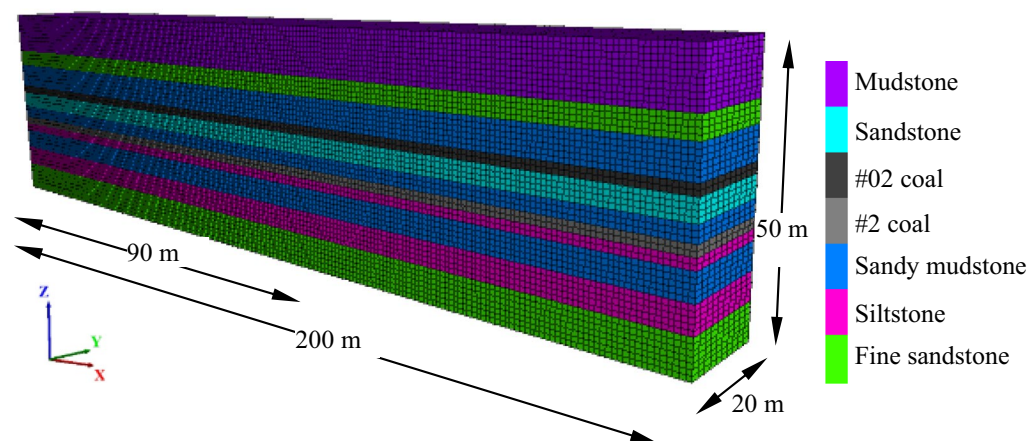


Fig. 5. Numerical calculation model.

Rock formation	Bulk modulus (GPa)	Shear modulus (GPa)	Density ($\text{kg}\cdot\text{m}^{-3}$)	Friction angle ($^{\circ}$)	Cohesion (MPa)	Tensile strength (MPa)
Sandy mudstone	3.8	2.6	2350	32	3.3	2.4
Fine sandstone	11.3	6.8	2500	34	3.1	2.7
Mudstone	3.6	2.1	2300	32	2.3	2.2
Sandstone	9.2	3.2	2400	32	2.6	2.3
Coal	1.3	1.1	1600	28	1.8	0.75
Siltstone	13.3	10.8	2600	35	4.9	2.9

Table 1. Mechanical parameters of the rock strata.

stress deviator concentration is located at the boundary of the coal pillar and gradually decreases with increasing depth.

By comparing Fig. 6a–c, it can be seen that when the width of the coal pillar is narrow, the influence range of the stress deviator below the coal pillar is relatively small, but the concentration is more obvious. When the width of the coal pillar is large, the influence range of the stress deviator below the coal pillar gradually increases, but the concentration gradually eases, and the value of J_2 below the coal pillar gradually decreases.

These figures demonstrate that the selection of coal pillar width for coal seam mining will directly affect the magnitude and distribution of the stress deviator. When the width of the coal pillar is smaller, the concentration of stress deviator is more obvious. The more nonuniform the stress of the rock mass is, the greater the distortion energy, and the worse the stability.

Meanwhile, these charts indicate that when the width of the coal pillar increases from 10 to 20 m, the peak value of J_2 decreases from 66.6 MPa² to 48.2 MPa², a significant decrease. When the width of the coal pillar increases from 20 to 30 m, the peak value of J_2 decreases from 48.2 MPa² to 44.6 MPa², a relatively small decrease.

Transmission of the stress deviator along the horizontal direction

When the width of the coal pillar is varied, the stress deviator will show a different distribution. To study the horizontal transmission of the stress deviator below the coal seam mining process, stress deviator distribution curves at the locations of $z=0$ m, $z=5$ m, $z=10$ m, $z=15$ m, $z=20$ m and $z=25$ m below the coal pillar are selected, as shown in Fig. 7. The relationship between the peak of stress deviator and its position with width of coal pillar (D) is shown in the upper right corner of each graph in Fig. 7.

According to Fig. 7, the stress deviator of the shallow surrounding rock ($z \leq 10$ m) is generally symmetrically distributed in an “M-shaped” bimodal pattern: As x increases, the curve at each depth of the gob floor first slowly decreases and then rapid increase at the boundary of the coal pillar. At $x=0$ m (the centerline of the coal pillar), the curve shows a turning point and slowly rises and then suddenly drops at the boundary of the opposite side coal pillar. At the shallow surrounding rock ($z \leq 10$ m), the peak of J_2 is near the boundary of the coal pillar, and the inflection point of the curve is located at the centerline of the coal pillar.

In the deep surrounding rock ($z \geq 10$ m), the stress deviator curve generally shows a symmetrical “single peak” distribution: as x increases, the curve at each depth of the floor slowly decreases and reaches a minimum value below the boundary of the coal pillar and then gradually rises and reaches a maximum value at the centerline of the coal pillar before slowly decreasing.

As the vertical position z increases, the stress deviator generally shows a gradually decreasing trend. Taking $D=10$ m as an example, when z is 0 m, 5 m, 10 m, and 15 m, the maximum values of J_2 are 65.68, 36.38, 27.61, and 10.91 MPa², respectively, when $z=0$ m, the corresponding peak is located at $x=4$ m, while the J_2 peak at

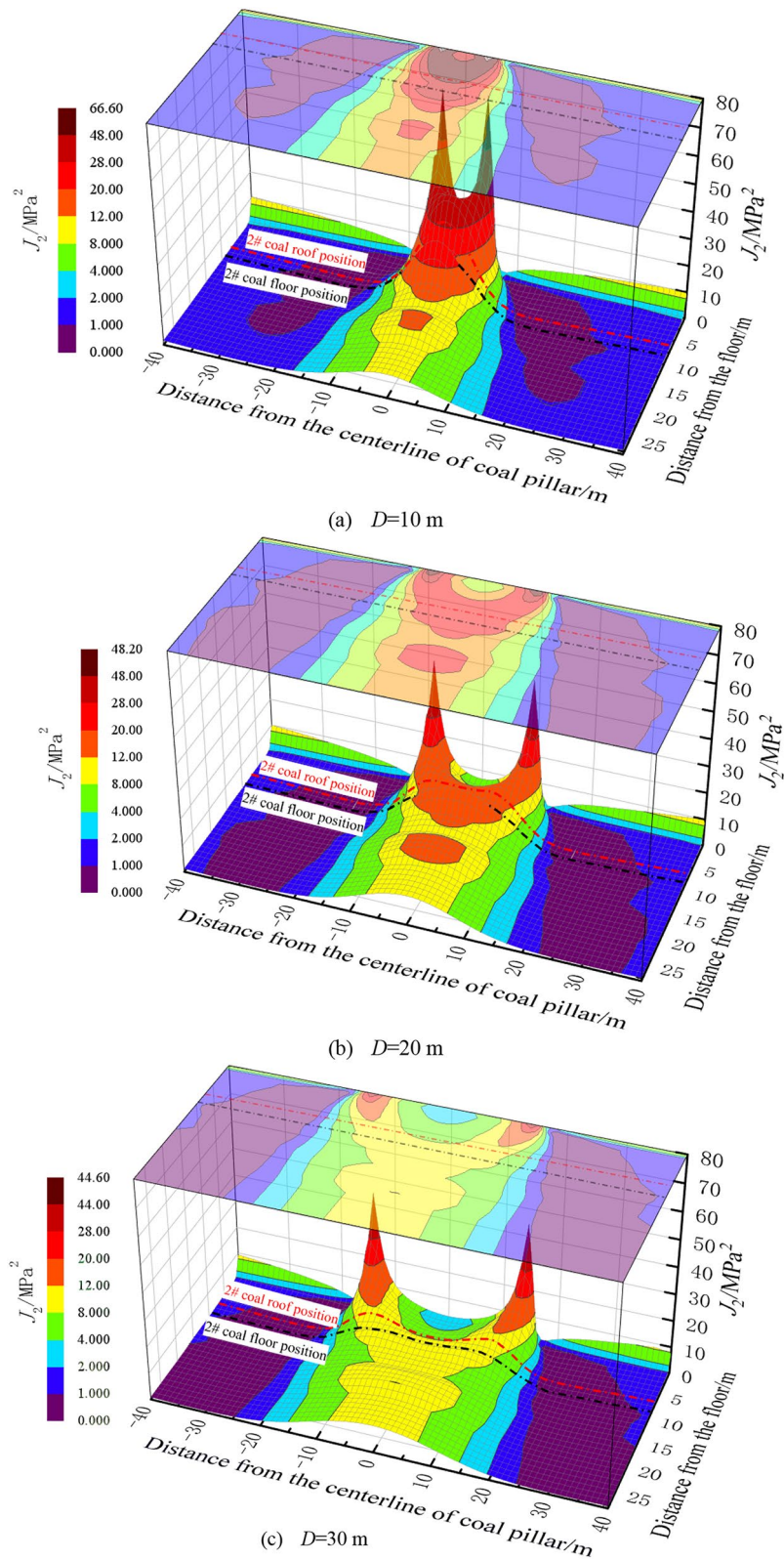


Fig. 6. Spatial distribution characteristics of stress deviator in the rock layer below the coal pillar.

other depths is located at $x=0\text{ m}$. This indicates that as the depth z increases, the peak value of J_2 decreases, and the peak positions at each depth gradually approach the centerline of the coal pillar ($x=0$).

Figure 7 illustrates the propagation pattern of the stress deviator in the horizontal direction, obtained through numerical simulation. The results indicate that the coal pillar width D and the vertical distance z from the base of

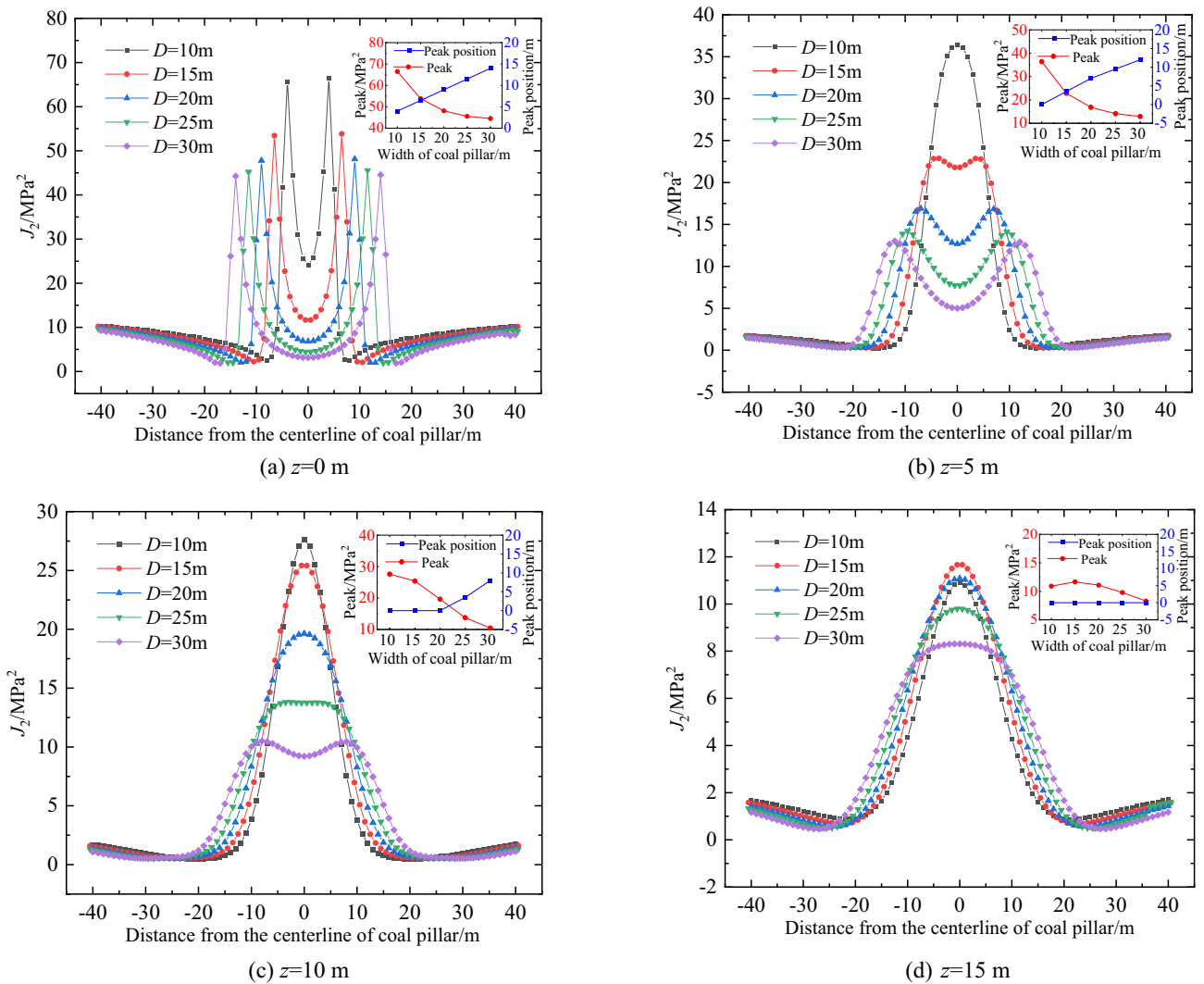


Fig. 7. Transmission of the stress deviator along the horizontal direction.

the pillar are the key parameters governing the transformation of the curve’s characteristic mode. By substituting these parameters into Eq. (7), derived from theoretical analysis, a consistent pattern is also observed analytically: A comparison between Figs. 4 and Fig. 7b shows that as the coal pillar width D increases, the peak zone of J_2 in the shallow surrounding rock shifts away from the central axis of the pillar. Moreover, the distribution of J_2 transitions from a single-peak to a double -peak form, with the magnitude of J_2 beneath the pillar gradually decreasing and its influence range slightly expanding.

The agreement between theoretical and numerical results confirms the validity of the theoretical derivation and the stress deviator distribution law, demonstrating the reliability of using the stress deviator as a guiding parameter in coal pillar design for mining engineering.

Transmission of the stress deviator along the vertical direction

Under different coal pillar widths, the transmission of the stress deviator along the vertical direction also varies, which is beneficial for further studying the evolution of the stress deviator. This section selected the centerline of the coal pillar ($x=0$), the boundary line of the coal pillar, and the distance from the boundary line of the coal pillar at 5 m and 10 m as the layout positions for vertical survey lines.

As shown in Fig. 8, there are significant differences in the transmission of the stress deviator along the depth depending on the position of the vertical measuring line. The stress deviator curve at the centerline of the coal pillar ($x=0$) shows a fluctuating trend of first increasing and then decreasing with increasing depth z . The stress deviator below the boundary of the coal pillar shows a decreasing trend with increasing depth z , and the deceleration gradually slows with increasing z . The stress deviator below the gob shows a sudden decreasing trend followed by a slow increase with increasing depth z .

By comparing Fig. 8a–d, when the width of the coal pillar is changed, although the transmission of the stress deviator is basically the same, there is a significant difference in the stress deviator value at different position, especially at the centerline of the coal pillar ($x=0$), at the boundary of the coal pillar, and below the gob near

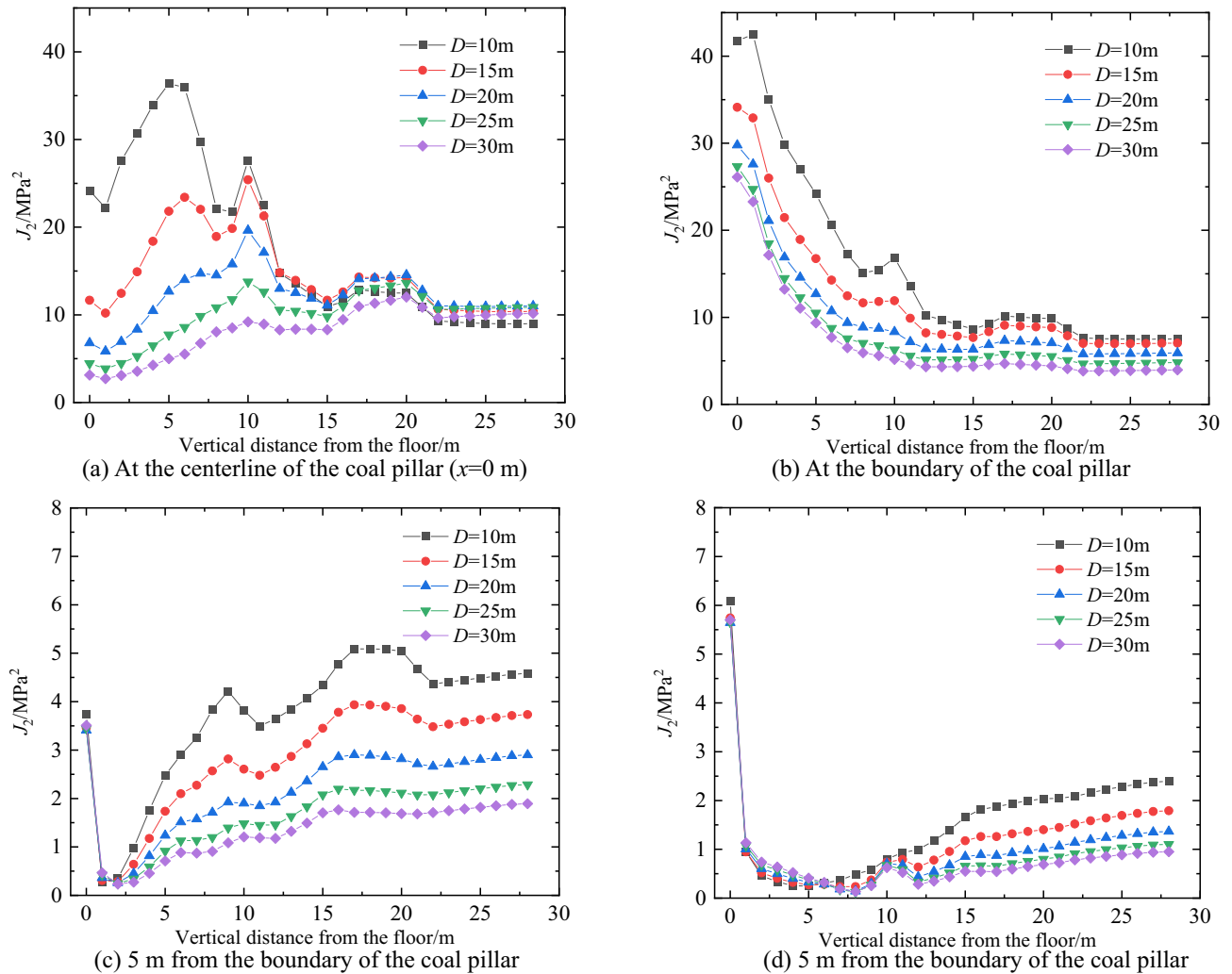


Fig. 8. Transmission of the stress deviator along the vertical direction.

the coal pillar, where this difference is more pronounced. This indicates that when the width of the coal pillar is narrow, the mining construction of the two panels will affect each other's stress distribution under their respective gob. Figure 8 shows that the influence range of the two panels is approximately 10–15 m below the gob, and when the width of the coal pillar is $D \geq 20$ m, the vertical transmission of the stress deviator is no longer significantly affected by the width of the coal pillar.

Reasonable selection and verification of coal pillar width

Reasonable selection of coal pillar width

The distribution characteristics of the stress deviator below the coal pillar also varies depending on the width of the coal pillar. This section explores the distribution characteristics of stress deviator under different coal pillar size effects, focusing on the specific practical engineering of coal seam mining in the Malan Mine. After the #02 coal seam (upper coal seam) of the Malan Mine is mined, the stability of the surrounding rock at the #2 coal seam (lower coal seam) under the influence of stress deviator is the key to ensuring safe construction.

Therefore, in this section, the distribution of the stress deviator in the surrounding rock at the roof of coal seam #2 is selected as the research object, which is the main basis for determining the reasonable width of coal pillar. The stress deviator value at this location will directly affect the stability of the surrounding rock during the mining process of the lower coal seam, as shown in Fig. 9.

Figure 9 shows the distribution of stress deviator at the roof of coal seam #2 below the coal pillar. Figure 9a indicates that as the width of the coal pillar increases, the peak value of the stress deviator at the floor continuously decreases, and the influence range of the stress deviator shows an expanding trend.

Figure 9a shows that as the coal pillar width increases from 10 to 20 m, the stress deviator decreases from 35.938 MPa² to 16.439 MPa², and the total stress deviator decreases by 19.50 MPa², a significant decrease. However, when the width of the coal pillar increases from 20 to 30 m, the stress deviator decreases from 16.439 MPa² to 12.180 MPa², and the total stress deviator decreases by 4.26 MPa², a small decrease. This indicates that when the

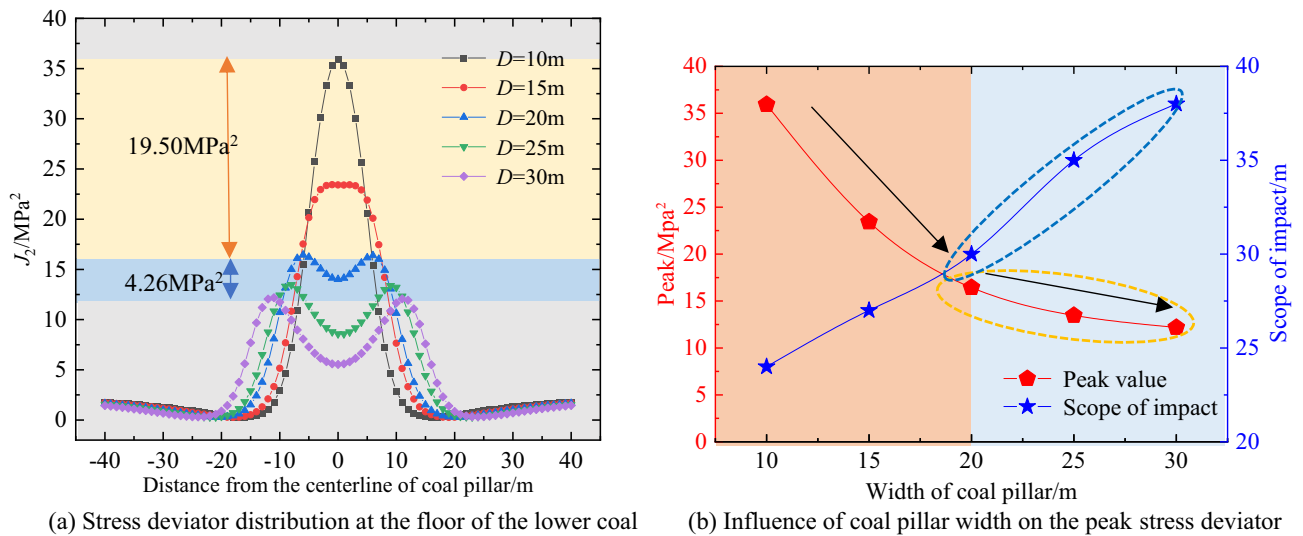


Fig. 9. Selection criteria for coal pillar width.

Rock strata	Strength of original rock (MPa)	Strength of model rock (MPa)	Strength ratio (MPa)	Material ratio		
				Sand	Cement	Gypsum
Topsoil	112.0	0.8	0.80	10	4	6
Sandy mudstone	30.85	0.22	0.23	9	1	9
Fine sandstone	92.30	0.66	0.67	10	3	7
Mudstone	31.61	0.23	0.23	9	1	9
Sandstone	79.36	0.57	0.58	9	2	8
Coal	18.19	0.13	0.15	10	1	9
Siltstone	77.83	0.56	0.58	9	2	8
Subsoil	112.0	0.8	0.80	10	4	6

Table 2. Physical and mechanical parameters of the rock strata.

width of the coal pillar is greater than 20 m, the increase in pillar width no longer has a significant impact on the stress deviator.

In Fig. 9b, the peak value and influence range of the stress deviator under various coal pillar width conditions were extracted. When the coal pillar width is 20 m, the curve of the peak stress deviator shows a significant turning point, and the slope of the curve decreases significantly, while the slope of the stress deviator influence range curve shows a slight increasing trend at this point.

This indicates that when the coal pillar width is 20 m, if the width of the coal pillar continues to increase, the impact of the coal pillar width on the stress deviator will no longer be significant but will actually increase the stress deviator range. In addition, from the perspective of rational resource utilization, blindly increasing the width of the coal pillar will also waste resources. Therefore, based on the above analysis, 20 m is determined as the reasonable width for the coal pillar in the 10605 and 10607 panels of the Malan Mine.

Design of similar simulation experiments

According to the similarity criterion, this section describes a study on the width of coal pillar in the 10607 panel of the Malan Mine using similarity simulation experiments³².

The test equipment located in the Mining Model Laboratory of China University of Mining and Technology (Beijing), with a size of 1400 mm × 200 mm × 1300 mm, is adopted. The geometric ratio of similar models is $\alpha_l = 100:1$. The bulk density ratio obtained from the proportioning test is $\alpha_\rho = 1.4:1$, and the strength similarity ratio of different rock layer materials is $\alpha_\sigma = \alpha_l \times \alpha_\rho = 140:1$. The ratio parameters of each rock layer are shown in Table 2. The ratio of cement to gypsum listed in the table represents the actual proportioning ratio, while the ratio coefficient specified under “sand” denotes the mass ratio of sand to the cementitious material (comprising cement and gypsum).

A similar model is laid according to the stratigraphic column in Fig. 1. To highlight the stress-strain characteristics at the coal pillar, the simulated length of the working face on both sides of the coal pillar is 50 cm, and the width of the coal pillar is 20 cm, as shown in Fig. 10. The top plate load is 10 MPa/140 = 71.4 kPa. There are lateral loading cylinders on both sides of the model, which apply lateral loads of 51.7 kPa each ($\lambda = 0.8$). The

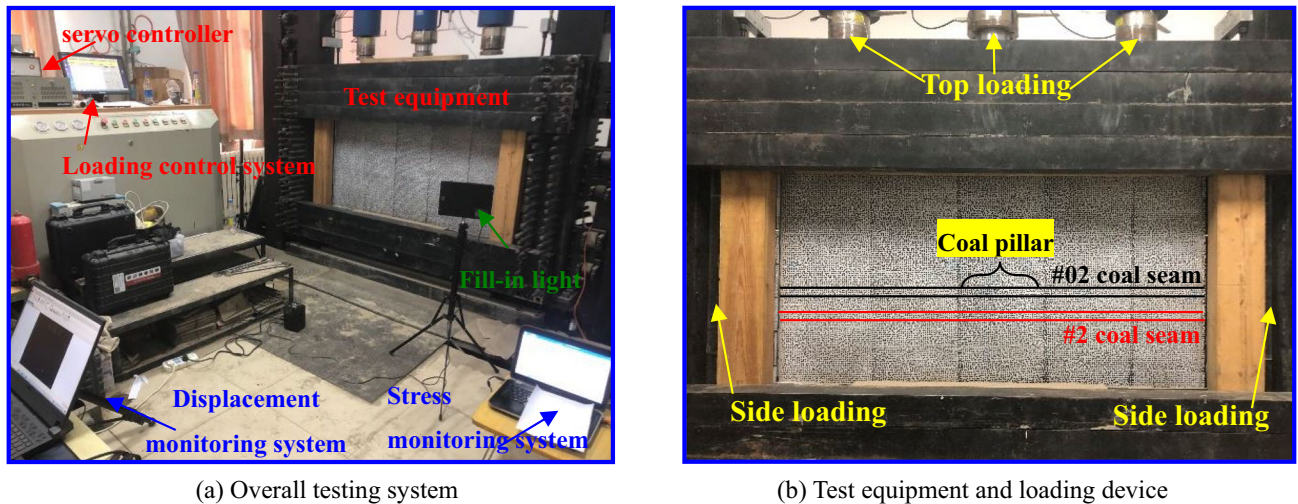


Fig. 10. Preparation of similar simulation experiment.

model adopts the plane stress assumption. 50 cm of simulated gob are mined on both sides of the #02 coal seam, with 5 cm/step, and a coal pillar with a width of 20 cm is left in the middle.

Results of similar simulation tests

Based on the relevant calculations of the stress deviator distribution characteristics mentioned above, in similar simulation experiments, it is proposed to leave a coal pillar width of 20 cm in the experiment. The vertical and horizontal stress distribution curves at 1.5 cm below the coal pillar are shown in Fig. 11a,b. The overall movement displacement of the surrounding rock in the mining area is recorded by DIC (digital image correlation)³³, and the displacement contour plot is shown in Fig. 11c.

According to Fig. 11a,b, there are slight differences in the vertical and horizontal stress values at each measuring point before mining, but the overall distribution is relatively uniform. The average vertical stress is 75.10 kPa, and the average horizontal stress is 61.16 kPa. The stress ratio calculation shows that the simulated stress is similar to the in situ stress. After the completion of mining on the left panel of the upper coal seam, because the load above the gob and the overlying rock cannot be directly transferred to the floor, the vertical stress and horizontal stress under the floor are reduced, and stress concentration occurs at the coal pillar. With the mining of the right panel, the vertical and horizontal stresses below the right gob also decrease, and the stress concentration at the coal pillar becomes more obvious. However, the final stress concentration coefficient is approximately 2.0. If the vertical stress of the coal pillar floor is considered the maximum principal stress, the x and y directions are the minimum and intermediate principal stresses, respectively. The stress deviator of the coal pillar floor is approximately 8–15 MPa², which is consistent with the numerical calculation, corresponding to a relatively safe range.

In addition, according to the displacement map of similar simulations (Fig. 11c), when the coal pillar is selected to be 20 m, the displacement in the coal pillar area (within the red dashed line) is mostly 0.1 mm (i.e., the actual displacement is within 10 cm), and the deformation of the surrounding rock in the coal pillar area is relatively small, resulting in a good stability.

The above results show that the selection of a 20 m width coal pillar can effectively ensure the safety and stability of the lower coal seam during the mining of close coal seams.

Field application

Through theoretical, numerical calculations, and physical model experiments, a coal pillar of 20 m was selected between the 10605 and 10607 panels. Figure 12 shows the roadway section and drilling observation results during the mining of the #2 coal seam (lower coal seam). The roadway is located below the 10607 panel and is 20 m away from the boundary of the coal pillar.

According to the field investigation observation results of the boreholes below the coal pillar, when the coal pillar is selected to be 20 m, the stability of the surrounding rock of the mining area floor is good, there are fewer regenerated cracks in the floor and two sides of surrounding rocks, and the overall integrity of the surrounding rock is good. In addition, the deformation of the roadway below the residual coal pillar is relatively small, the deformation during the observation period is within 10 cm, and there is no occurrence of surrounding rock peeling or collapse.

This indicates that selecting a 20 m coal pillar in the upper coal mining area through the distribution characteristics of the stress deviator effectively suppresses the plastic development of the floor, protects the integrity of the lower coal seam below the coal pillar, and ensures the safe and stable mining of the lower coal seam. The application of stress deviator is beneficial for improving the theory of mine pressure.

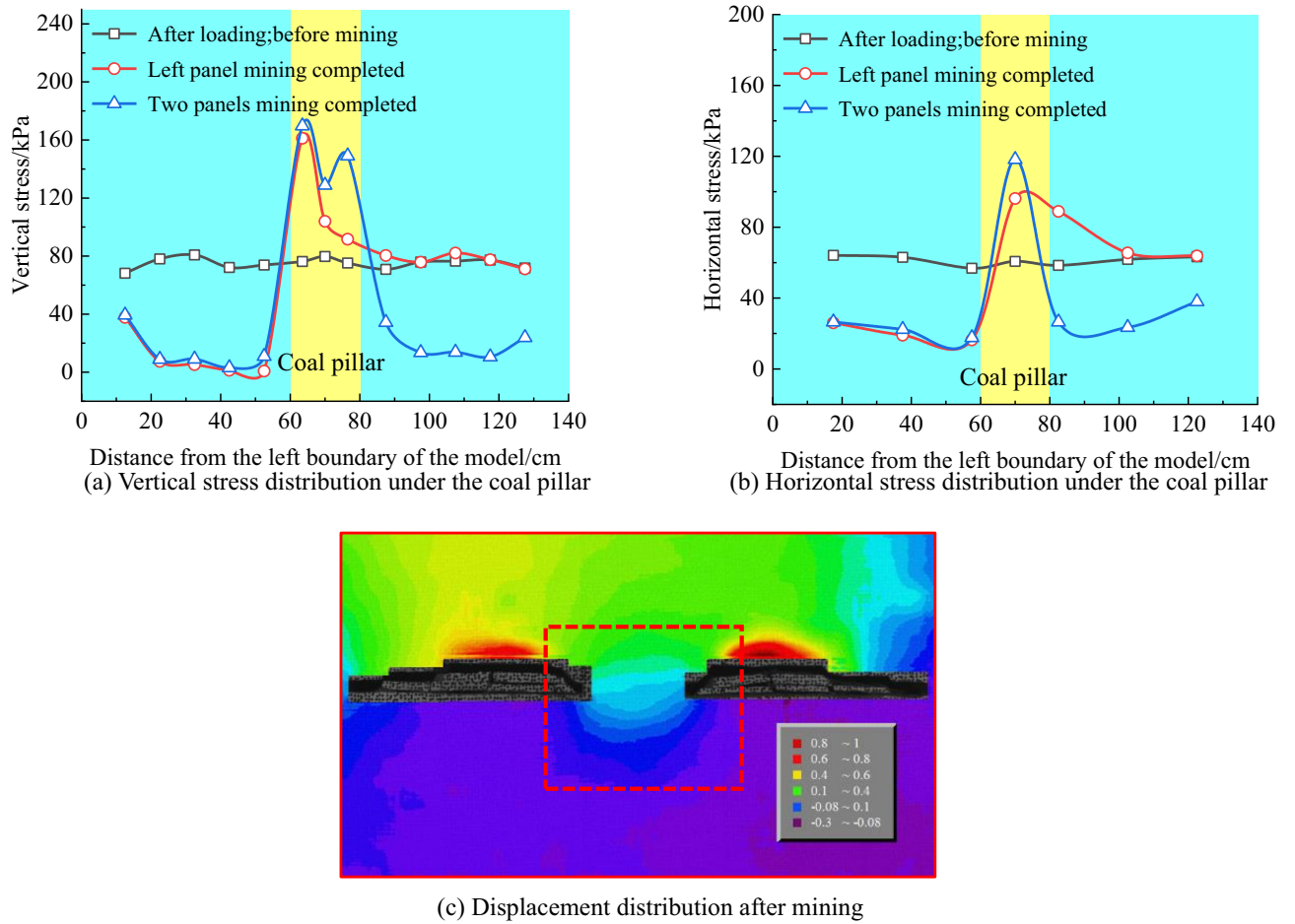


Fig. 11. Results of similar simulation tests.



Fig. 12. Field investigation and drilling observation.

Discussion

The above research indicates that the magnitude of the stress deviator in the rock mass beneath the coal pillar have a significant influence on the deformation energy and stability of the surrounding rock. Therefore, the study of the stress deviator is of certain significance. However, the following aspects should be further discussed:

- (1) This paper investigates the stress deviator of the rock mass beneath the coal pillar through specific engineering examples, with a focus on field design. Accordingly, the analysis centers on the influence of coal pillar width. However, other factors, such as the initial in-situ stress and rock formation characteristics, may also have important effects on the stress deviator, which requires further investigation.

- (2) The closely spaced coal seams discussed in this paper are relatively typical and common, which gives the study a certain degree of general applicability. For the rock mass near the roof of mining areas and geological structure belts, the numerical results of the stress deviator second invariant (J_2) may still offer engineering reference value. However, due to the fragmented and discontinuous nature of the rock mass in these areas, the basic assumptions of the theoretical analysis in this study may not be entirely applicable.
- (3) Compared with vertical and horizontal stress components, J_2 is a comprehensive indicator that reflects rock energy under multi-directional stress conditions. Therefore, J_2 has the potential to serve as a useful indicator not only in the design of mining layouts, but also in studies related to roadway and tunnel surrounding rock, as well as slope stability.

Conclusion

- (1) Through a mechanical model of the coal pillar floor and an expression of the coal pillar floor stress, a calculation formula for the stress deviator of a single coal pillar floor was derived. Through analysis, it was found that the magnitude of the concentrated load in the coal pillar area and the width of the coal pillar are the main factors affecting the distribution of the stress deviator.
- (2) Both theoretical and numerical calculations indicate that the stress deviator distribution below the coal pillar exhibits a symmetrical "Y-shaped" distribution. The main area of stress deviator concentration is located at the boundary of the coal pillar, and as the depth increases, the peak value of the stress deviator gradually decreases, and the concentration area gradually approaches the centerline of the coal pillar.
- (3) When the width of the coal pillar between the two gobs is narrow, the influence range of the stress deviator below the coal pillar is relatively small, but the concentration phenomenon is more obvious. As the width of the coal pillar increases, the influence range of the stress deviator below the coal pillar gradually increases, but the concentration gradually eases, and the peak value of stress deviator below the coal pillar gradually decreases.
- (4) Based on the influence of coal pillar width on the distribution characteristics of stress deviator in the floor, the width of the coal pillar for the upper coal seam during coal seam mining in the Malan Mine was determined. Physical model experiments and on-site observations found that when the coal pillar was selected to be 20 m, the development of cracks in the surrounding rock below the coal pillar was lessened, and the stability was better. This also reflects the potential of stress deviator in theoretical research and guiding engineering practice.

Data availability

The data that support the findings of this study are available from the corresponding author upon reasonable request.

Received: 19 March 2025; Accepted: 12 May 2025

Published online: 20 May 2025

References

1. Brady B. H. G., Brown E. T. *Rock Mechanics for Underground Mining* (2004).
2. Suchowerska, A. M., Merifield, R. S. & Carter, J. P. Vertical stress changes in multi-seam mining under supercritical longwall panels. *Int. J. Rock Mech. Min. Sci.* **61**, 306–320. <https://doi.org/10.1016/j.ijrmms.2013.02.009> (2013).
3. Suchowerska, A. M., Carter, J. P. & Merifield, R. S. Horizontal stress under supercritical longwall panels. *Int. J. Rock Mech. Min. Sci.* **70**, 240–251 (2014).
4. Das, A. J., Mandal, P. K., Paul, P. S. & Sinha, R. K. Generalised analytical models for the strength of the inclined as well as the flat coal pillars using rock mass failure criterion. *Rock Mech. Rock Eng.* **52**(10), 3921–3946. <https://doi.org/10.1007/s00603-019-0178-7> (2019).
5. Torano, J., Diez, R. R., Cid, J. R. & Barciella, M. C. FEM modeling of roadways driven in a fractured rock mass under a longwall influence. *Comput. Geotech.* **29**(6), 411–431. [https://doi.org/10.1016/S0266-352X\(02\)00006-X](https://doi.org/10.1016/S0266-352X(02)00006-X) (2002).
6. Zhang, J. & Guo, L. Peridynamic investigation on crack propagation mechanism of rock mass during excavation of tunnel group in cold regions. *Mech. Adv. Mater. Struct.* **31**(14), 3061–3076. <https://doi.org/10.1080/15376494.2023.2169791> (2024).
7. Tan, Y. L., Zhao, T. B. & Xiao, Y. X. In situ investigations of failure zone of floor strata in mining close distance coal seams. *Int. J. Rock Mech. Min. Sci.* **47**(5), 865–870. <https://doi.org/10.1016/j.ijrmms.2009.12.016> (2010).
8. Brady, B. H. & Brown, E. T. *Rock Mechanics: For Underground Mining* (Springer Science & Business Media, 1993).
9. Qian, J. et al. Optimization of ore pillar recovery based on weighting combined with uncertainty measurement theory. *J. Geophys. Eng.* **21**(6), 1822–1833. <https://doi.org/10.1093/jge/gxae108> (2024).
10. Sun, J., Wang, L. & Zhao, G. Stress distribution and failure characteristics for workface floor of a tilted coal seam. *KSCE J. Civ. Eng.* **23**(9), 3793–3806. <https://doi.org/10.1007/s12205-019-0786-7> (2019).
11. Cheng, X., Wen, H., Xu, Y., Fan, S. & Ren, S. Environmental treatment technology for complex coalfield fire zone in a close distance coal seam: A case study. *J. Therm. Anal. Calorim.* <https://doi.org/10.1007/s10973-020-10302-z> (2020).
12. Wang, X. et al. Numerical investigation of coal pillar damage mechanisms for various width-to-height ratios. *Sci. Rep.* **15**(1), 2705. <https://doi.org/10.1038/s41598-025-85554-6> (2025).
13. Li, J. The coal pillar design method for a deep mining roadway based on the shape of the plastic zone in surrounding rocks. *Arab. J. Geosci.* **13**(12), 454. <https://doi.org/10.1007/s12517-020-05501-9> (2020).
14. Zhu, S. et al. Determination of width of sectional coal pillars in the working face of burst-prone inclined thick coal seams. *Shock Vib.* **2022**(1), 4186791. <https://doi.org/10.1155/2022/4186791> (2022).
15. He, W., He, F. & Zhao, Y. Field and simulation study of the rational coal pillar width in extra-thick coal seams. *Energy Sci. Eng.* **8**(3), 627–646. <https://doi.org/10.1002/ese3.538> (2020).
16. Shan, R. et al. Research on the mechanism of asymmetric deformation and stability control of near-fault roadway under the influence of mining. *Eng. Fail. Anal.* **127**, 105492. <https://doi.org/10.1016/j.engfailanal.2021.105492> (2021).
17. Li, Z. L. et al. Study on the influence of the fault dip angle on the stress evolution and slip risk of normal faults in mining. *Bull. Eng. Geol. Environ.* <https://doi.org/10.1007/s10064-021-02149-x> (2021).

18. Yu, L., Peng, K., Luo, S., Wang, Y. & Luo, K. Failure process and characteristics of deep concrete-supported arch tunnel under true-triaxial stress. *Theoret. Appl. Fract. Mech.* **130**, 104295. <https://doi.org/10.1016/j.tafmec.2024.104295> (2024).
19. Si, X. et al. Influences of maximum principal stress direction and cross-section shape on tunnel stability. *J. Rock Mech. Geotechn. Eng.* <https://doi.org/10.1016/j.jrmge.2024.10.003> (2024).
20. Luo, Y., Huang, J., Wu, W., Si, X. & Zhu, C. Saturation effect on storage-dissipation properties and failure characteristics of red sandstone: Energy mechanism of water in preventing rockburst. *Int. J. Coal Sci. Technol.* **12**(1), 1–19. <https://doi.org/10.1007/s40789-025-00770-9> (2025).
21. Xie, S. R., Jiang, Z. S., Chen, D. D., Wang, E. & Lv, F. A new pressure relief technology by internal hole-making to protect roadway in two sides of deep coal roadway: A case study. *Rock Mech. Rock Eng.* **56**(2), 1537–1561. <https://doi.org/10.1007/s00603-022-03135-9> (2023).
22. Chen, D. D. et al. The J_2 evolution model and control technology of the main roadway surrounding rock under superimposed influence of double-coal seam mining. *Sci. Rep.* **13**(1), 17569. <https://doi.org/10.1038/s41598-023-44136-0> (2023).
23. Li, Z. L., Shan, R. L., Wang, C. H., Yuan, H. H. & Wei, Y. H. Study on the distribution law of stress deviator below the floor of a goaf. *Geomech. Eng.* **21**(3), 301–313. <https://doi.org/10.1007/s12665-021-09891-1> (2020).
24. Shan, R. et al. Study on the distribution characteristics of stress deviator in the surrounding rock when mining closely spaced coal seams. *Environ. Earth Sci.* **80**(17), 1–18. <https://doi.org/10.12989/gae.2020.21.3.301> (2021).
25. Wang, Y., Jing, H., Su, H. & Xie, J. Effect of a fault fracture zone on the stability of tunnel-surrounding rock. *Int. J. Geomech.* **17**(6), 04016135. [https://doi.org/10.1061/\(ASCE\)GM.1943-5622.0000837](https://doi.org/10.1061/(ASCE)GM.1943-5622.0000837) (2017).
26. Tian, M. et al. Physical model experiment of surrounding rock failure mechanism for the roadway under deviatoric pressure form mining disturbance. *KSCE J. Civ. Eng.* <https://doi.org/10.1007/s12205-020-1540-x> (2020).
27. Kroon, M. & Faleskog, J. Numerical implementation of a J_2 and J_3 dependent plasticity model based on a spectral decomposition of the stress deviator. *Comput. Mech.* **52**(5), 1059–1070. <https://doi.org/10.1007/s00466-013-0863-6> (2013).
28. Sun, Y. J., Xie, S. R., Li, S. J., Song, B. H. & Huang, X. Reasonable location of roadway in coal pillar area under different layer located key blocks and its surrounding rock control. *J. China Univ. Min. Technol.* **04**, 694–701. <https://doi.org/10.13247/j.cnki.jcunt.000550> (2016) (In Chinese).
29. Shan, R. et al. Study on distortion energy and stability of gob floor based on stress deviator field. *Energy Sci. Eng.* **10**(8), 2756–2771. <https://doi.org/10.1002/ese3.1165> (2022).
30. Xu, L., Wei, H. X., Xiao, Z. & Li, B. Engineering cases and characteristics of deviatoric stress under coal pillar in regional floor. *Rock Soil Mech.* **02**, 561–568. <https://doi.org/10.16285/j.rsm.2015.02.036> (2015) (In Chinese).
31. Zhang, B. S. *Study on the Surrounding Rock Control Theory and Technology of Ultra-Close Multiple-Seams Mining* (Taiyuan University of Technology, 2008) (In Chinese).
32. Chen, J., Chen, J., Rui, Y. & Pu, Y. Joint inversion of AE/MS sources and velocity with full measurements and residual estimation. *Rock Mech. Rock Eng.* **57**(9), 7371–7386. <https://doi.org/10.1007/s00603-024-03917-3> (2024).
33. Guo, T. et al. Mechanical characteristics and fracturing behavior of rock-concrete composite specimens with two pre-existing parallel flaws under uniaxial compression based on AE and DIC systems. *Theor. Appl. Fracture Mech.* **136**, 104866. <https://doi.org/10.1016/j.tafmec.2025.104866> (2025).

Acknowledgements

This work was supported by the National Natural Science Foundation of China (Grant No. 52274148), the National Science Foundation of Hebei Province (Grant No. E2023402103), Science Research Project of Hebei Education Department (QN2025247) and Handan Science and Technology R&D Project (23422093047).

Author contributions

Li Zhaolong: Investigation, Software, Writing. Li Jun: Conceptualization, Supervision. Shan Renliang: original draft. Liu Jingju: Data curation, Writing. Tong Xiao: Investigation. Liu Nan: Visualization.

Competing interests

The authors declare no competing interests.

Additional information

Correspondence and requests for materials should be addressed to Z.L.

Reprints and permissions information is available at www.nature.com/reprints.

Publisher's note Springer Nature remains neutral with regard to jurisdictional claims in published maps and institutional affiliations.

Open Access This article is licensed under a Creative Commons Attribution-NonCommercial-NoDerivatives 4.0 International License, which permits any non-commercial use, sharing, distribution and reproduction in any medium or format, as long as you give appropriate credit to the original author(s) and the source, provide a link to the Creative Commons licence, and indicate if you modified the licensed material. You do not have permission under this licence to share adapted material derived from this article or parts of it. The images or other third party material in this article are included in the article's Creative Commons licence, unless indicated otherwise in a credit line to the material. If material is not included in the article's Creative Commons licence and your intended use is not permitted by statutory regulation or exceeds the permitted use, you will need to obtain permission directly from the copyright holder. To view a copy of this licence, visit <http://creativecommons.org/licenses/by-nc-nd/4.0/>.

© The Author(s) 2025